ARTICLE NO. 78-1508R

Properties of Aspect-Ratio-4.0 Rectangular Jets in a Subsonic Crossflow

Robert P. Weston*
NASA Langley Research Center, Hampton, Va.
and
Frank C. Thames†
Vought Corporation, Dallas, Texas

A series of wind-tunnel and laboratory tests were conducted at the NASA Langley V/STOL tunnel facility to determine both the detailed structure and the induced effects of aspect-ratio-4.0 rectangular jets, both in a subsonic crosswind and in quiescent conditions. Wind-tunnel tests were conducted on both blunt (nozzle major axis normal to freestream) and streamwise (nozzle major axis parallel to freestream) nozzle orientations for jet injection angles in the range 15 deg $\leq \delta_j \leq$ 90 deg, at jet-to-crossflow velocity ratios of 4, 8, and 10. Results indicate that the blunt-nozzle induced effects are more significant than those produced by comparable streamwise-oriented jets and that both the flowfield structure and induced effects of streamwise-oriented rectangular jets are quite similar to those created by round jets. Additionally, it is shown that significant differences exist in the vortex flowfields generated by the same rectangular nozzle mounted in two different test hardware configurations.

Nomenclature

a,b,c,d	= curve fitting parameters
C_p	= static pressure coefficient
D_e	= equivalent jet diameter, cm (in.)
e_1,e_2,e_3	= unit vectors (see Fig. 11)
h	= vortex spacing, cm (in.)
M	= jet exit Mach number
R	= jet-to-crossflow velocity ratio
r	= distance in vortex coordinate system (see Fig. 11)
U,V,W	= X, Y, Z components of velocity; denotes components in wind-tunnel system when no subscript is used, m/s (ft/s)
X,Y,Z	= Cartesian coordinate system; denotes wind-tunnel coordinate system when no subscript is used (see Fig. 3)
x,y,z	= distances along X, Y, and Z axes, m (ft)
x',z'	= trajectory origin offsets [see Eqs. (2) and (3), respectively]
$\bar{z}$	= Z_v coordinate of vortex center
β	= diffusion constant [see Eq. (5)]
Γ	= strength of each vortex, m^2/s (ft^2/s)
γ	= dimensionless variable, $\gamma = \Gamma/2D_eU_\infty$
δ_j	= jet injection angle, deg
θ	= angle of inclination, deg
ω	= vorticity, s^{-1}

Subscripts

c	= refers to jet centerline
j	= refers to condition at jet orifice
o	= refers to integrated value for one Lamb vortex
v	= refers to vortex curve
∞	= refers to crossflow condition
$1,2$	= refers to Lamb vortex numbering

Presented as Paper 78-1508 at the AIAA Aircraft Systems and Technology Conference, Los Angeles, Calif., Aug. 21-23, 1978; submitted Sept. 25, 1978. Reprints of this article may be ordered from AIAA Special Publications, 1290 Avenue of the Americas, New York, N.Y. 10019. Order by Article No. at top of page. Member price $2.00 each, nonmember, $3.00 each. **Remittance must accompany order.**

Index category: Jets, Wakes, and Viscid-Inviscid Flow Interactions.

*Aerospace Engineer, Low-Speed Aerodynamics Branch, Subsonic-Transonic Aerodynamics Division.

†Engineering Specialist. Member AIAA.

I. Introduction

THE physical situation in which a high-speed turbulent jet is injected into a subsonic crossflow at relatively large angles occurs in a number of practical problems. From an aerodynamic point of view, the basic interest lies in the transition from thrust-supported to wingborne flight of a V/STOL aircraft. The physical phenomena arising from the jet/crossflow interaction are quite complex and always three-dimensional in nature. Viscous effects play a large role in the interaction. For these reasons, direct analytical/computational efforts to study the problem have been almost nonexistent. Most of what is known about the jet/crossflow interaction has therefore come from testing. Thus, although the precise details of the interaction are not known, there has emerged over the years a fairly accurate physical description of the qualitative nature of the interaction.

As the high-velocity jet leaves the nozzle exit, the jet momentum is sufficient to penetrate the crossflow in an essentially inviscid fashion. At this stage, the jet appears initially as a solid obstruction to the oncoming crossflow. However, as the jet penetrates the crossflow, it entrains low-momentum fluid from the crossflow. In addition, viscous effects begin to erode the momentum of the primary jet flow. As the net velocity in the jet plume is lost, it begins to deflect in the direction of the crossflow and eventually becomes parallel to the freestream flow. This event nominally occurs at 10-15 equivalent jet diameters downstream of the orifice. Downstream of this point, it is very difficult to detect the primary jet plume experimentally.

The other major feature of the interaction is a pair of contrarotating vortices which form near the nozzle orifice and proceed downstream slightly below and on the lee side of the primary jet flow. In contrast to the primary flow, these vortices are quite persistent and have been observed as far as 1000 jet diameters downstream of the jet exit.[1] In summary, the jet/crossflow interaction is a composite of three phenomena: a blockage effect which occurs early in the interaction, the entrainment of crossflow fluid by the jet, and the formation of a pair of long-lived contrarotating vortices.

The round jet in a crossflow has been studied over the years by a number of investigators. In the earlier efforts, studies were concentrated on measuring the path of the jet (locus of maximum total pressure) and its induced pressure field on

some local geometry. The usual experimental apparatus consisted of a nozzle orifice mounted on a large flat plate or reflection plane. An excellent summary of these earlier efforts is given in Ref. 2 and in the references which it contains. In the late 1960's and early 1970's, researchers began measuring the details of the contrarotating vortex structures. Early work in this area was reported by Pratte and Baines,[1] Thompson,[3] and Kamotani and Greber.[4]

Also early in the 1970's, Fearn and Weston began, under NASA sponsorship, an extensive study of the round jet in a crossflow. A series of tests were conducted on round jets at various jet-to-crossflow velocity ratios, R, and jet injection angles, δ_j. The primary emphasis of the work was the detailed measurement and analysis of the jet plume and contrarotating vortex flows. Fearn and Weston developed two empirical models to extract vortex strength and spacing information from their data. They also showed that the jet plume (or jet centerline) and vortex curves obey a similarity rule.[5] Other results of their work appear in a series of NASA documents and conference papers.[6-8]

The current study on aspect-ratio-4.0 rectangular jets is an extension of Fearn's and Weston's work on circular jets. The purpose of the study was to develop a consistent base data set for rectangular nozzles and a potential-flow analytical model capable of calculating the induced effects of the jet/crossflow interaction for V/STOL aircraft in transition flight. This paper presents the results of the experimental investigation of the flowfields and a discussion of the data reduction and analysis procedures, as well as the conclusions.

II. Description of Tests

Wind-Tunnel Tests

Test Installations

The jet-in-crossflow wind-tunnel tests were conducted in the NASA Langley Research Center V/STOL tunnel. Two test installations were utilized: a 12 D_e by 24 D_e reflection plane for large-angle injections (45 deg $\leq \delta_j \leq$ 90 deg) of both the blunt (major nozzle axis normal to freestream) and streamwise (major axis parallel to freestream) oriented jets (Fig. 1), and a faired-body installation suitable for small-angle injection (15 deg $\leq \delta_j \leq$ 45 deg) of blunt oriented jets. The jets were created by expanding high-pressure air into a circular plenum (with screens), through a circular-to-rectangular transition fairing, and into a constant-area duct curved to develop the appropriate injection angles. The plenum and duct assemblies lie inside the airfoil-shaped fairing located under the plate installation (Fig. 1) and inside the faired body itself in the low-angle installation (Fig. 2). The high-pressure air supply was heated so that the nozzle flows exited at tunnel static conditions. This was done to eliminate buoyancy effects from the data. The jet velocities were controlled by setting the stagnation pressure and temperature in the plenum chamber and allowing the air to expand isentropically.

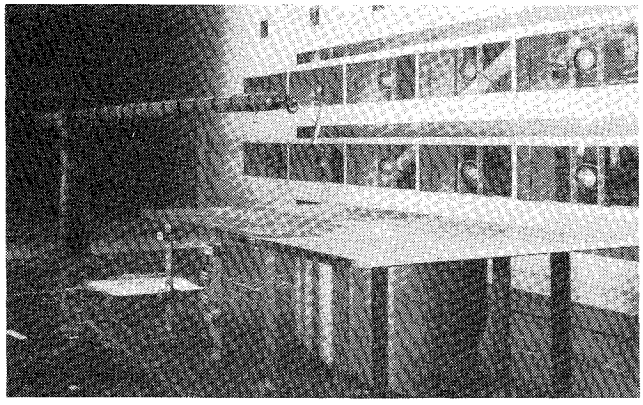

Fig. 1 Reflection plane test installation in the Langley V/STOL tunnel.

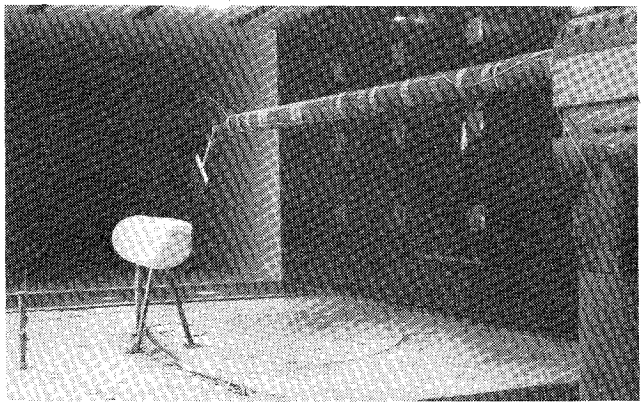

Fig. 2 Faired body test installation in the Langley V/STOL tunnel.

Test variables included nozzle configuration (blunt or streamwise), jet-to-freestream velocity ratio, R, and jet injection angle, δ_j. Two primary types of data were acquired: detailed jet/vortex flowfield measurements and surface static pressure distributions (reflection plane installation only). The test conditions are summarized in Table 1.

Instrumentation

The reflection plane was instrumented with 217 static pressure ports arranged in a rectangular matrix to measure the interference pressure field induced by the jet/crossflow interaction. The pressures were monitored with a ±17.4 kPa (±2.5 psid) transducer using conventional pressure scanning mechanisms.

A variety of quantities were measured in the air supply system. The more important of these were the total pressure and temperature measurements made in the plenum, as these were used to set the jet exit conditions. These total conditions were set, and the isentropic expansions to prescribed jet Mach numbers ($M=0.5$ for $R=4$ and $M=0.9$ for $R=8$, 10) were assumed to obtain the desired jet exit velocity. (The accuracy of this approach was validated in nozzle laboratory tests.) Fearn and Weston[6] have shown that varying jet exit Mach number for a constant R has an insignificant effect on the jet/crossflow interaction.

The details of the flowfield were measured with a rake containing seven hemispherical-tipped yaw-pitch probes. The individual probes were of the standard six-port variety, having a total and static port with four additional ports to detect flow angularity. Special procedures[6] were used to calibrate the probes to obtain flow angle and velocity measurement capability over a wide range of conditions. The flow angle resolution capability of the probes was determined to be ±1 deg; the dynamic pressure was accurate to within ±2.5% for angles less than 25 deg and ±5% elsewhere.

Table 1 Test conditions, $R=4$, 8, and 10

Test installation	Nozzle configuration	δ_j	Vortex data	C_p data
Reflection plane	Blunt	45	Yes	Yes
		60		
		75		
		90		
	Streamwise	60	No	
		75	Yes	
		90		
Faired body	Blunt	15		No
		30		
		45		

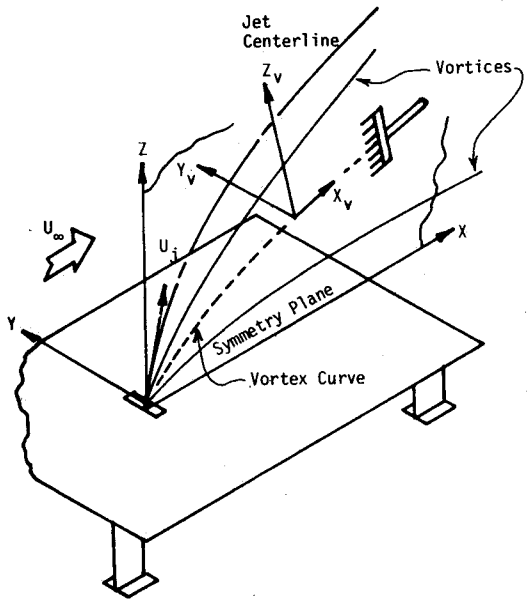

Fig. 3 Jet/crossflow interaction schematic.

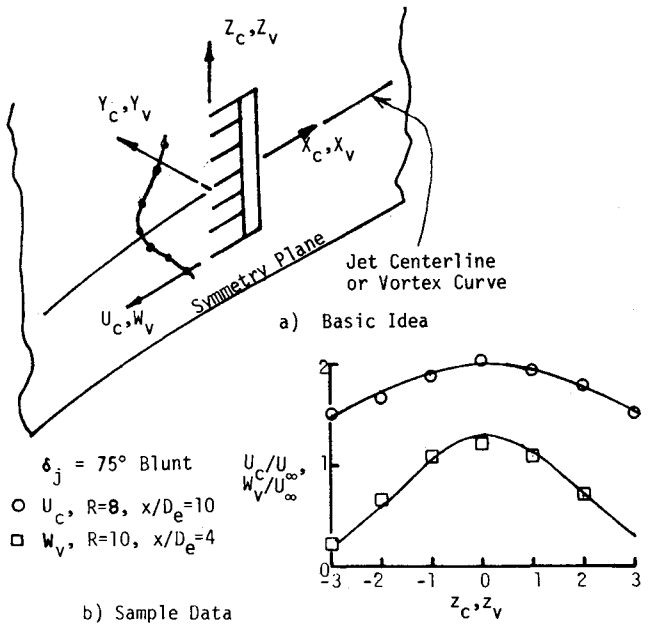

Fig. 4 Locating jet centerline and vortex curves.

Test Procedures

The major portion of the tunnel investigation was devoted to the acquisition of detailed velocity measurements in the jet plume and associated contrarotating vortex flows. The procedures used to acquire these data are described later. Detailed measurements were made with the velocity rake at a number of X/D_e stations downstream of the jet orifice, as illustrated in Fig. 3. At any given station, the rake was positioned so that the center probe lay approximately on and parallel to the jet centerline trajectory (locus of maximum total pressure). The U_c velocity components of the seven probes were monitored to locate the peak in the U_c component, which corresponds to the location of the jet centerline. This procedure is illustrated in Fig. 4. The rake was then lowered to initiate measurement of the vortex flows. The vortex curve (defined as the projection of the vortex trajectories onto the symmetry plane) was easily located by monitoring the W_v component of velocity, since this component has a peak along the line joining the two vortex centers, as shown in Fig. 4. Once the vortex curve was located, a lateral sweep was made to measure detailed velocities in the contrarotating vortex structure. A sample of this type of data is shown in Fig. 5, which gives a quantitative picture of the three velocity components. (The contours are of the U_v component which is normal to the paper.)

Laboratory Tests

In order to establish the nature of the initial jet flowfields, calibration tests were made on the nozzles used during the tests. Three types of data were acquired: 1) nozzle exit total pressure profiles, 2) true jet deflection angle measurements, and 3) nozzle jet decay data. The results of the nozzle angle tests showed, on the average, that the true jet angle deviated from the nominal set angle by ± 0.13 deg. The nozzle total pressure profile data indicated that the nozzles were operating in a satisfactory fashion with no large-scale boundary-layer effects. The jet decay (reduction of jet centerline total pressure with distance from the jet exit) data indicated that the rectangular jets decay much faster than circular jets of the same equivalent diameter. The faster decay rate is due primarily to increased viscous effects arising from the larger perimeter surface of the rectangular nozzles ($\approx 41\%$ greater).

III. Data Reduction and Analyses

Reflection Plane Test Results

Static Pressure Distributions

The reflection-plane static pressure distributions were acquired to quantify the induced effects of the jet/crossflow interaction. Contours of these measurements for both blunt

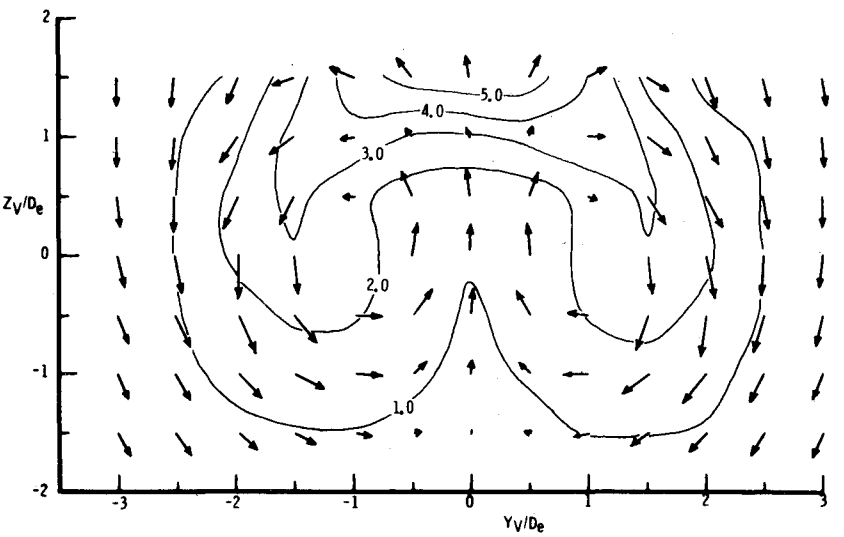

Fig. 5 Lateral vortex sweep data, $R = 10$, $\delta_j = 45$ deg blunt.

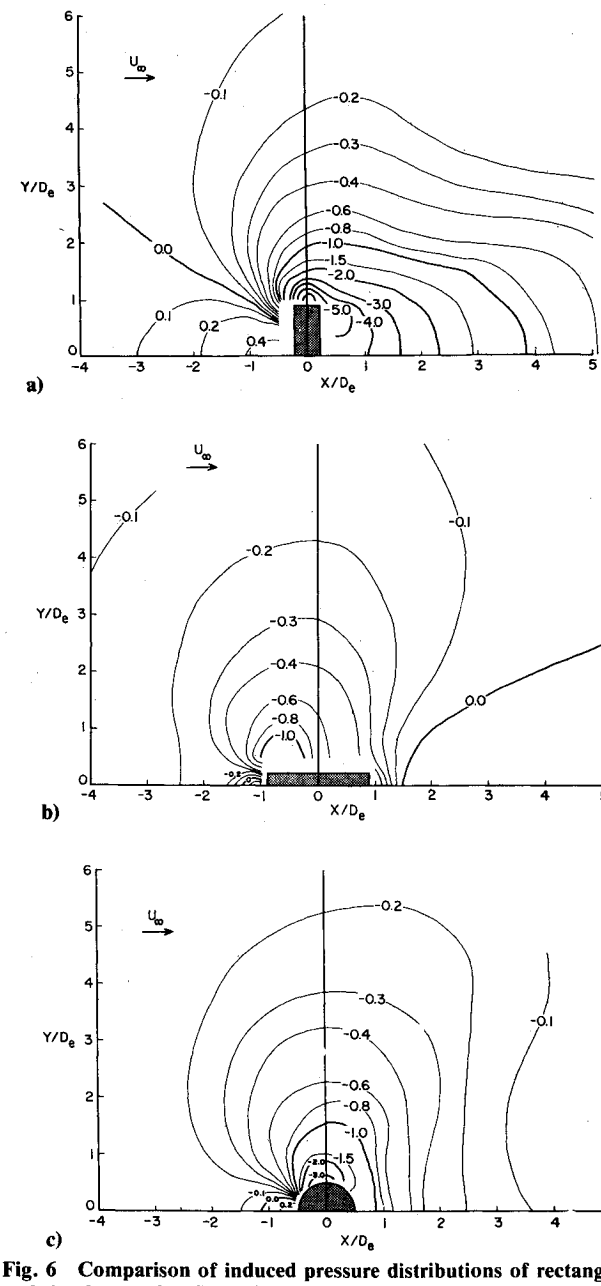

Fig. 6 Comparison of induced pressure distributions of rectangular and circular nozzles, $R = 4$, $\delta_j = 90$ deg.

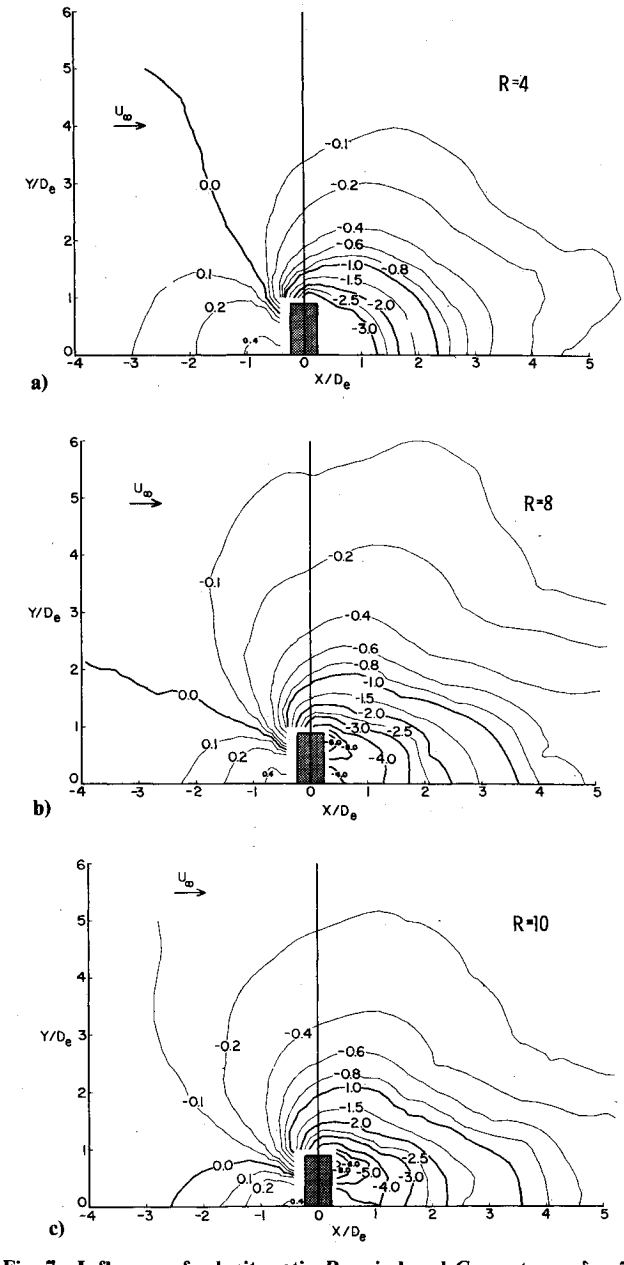

Fig. 7 Influence of velocity ratio R on induced C_p contours, $\delta_j = 75$ deg.

and streamwise orientations of the jets are given in Fig. 6, for a normally injected jet at $R = 4.0$. [The quantity contoured is actually $\Delta C_p = C_p$ (jet on) $- C_p$ (jet off).] The blunt nozzles are characterized by a significant low-pressure wake region, a region of positive pressure forward of the nozzle, and a region of low pressure which spread laterally from the sides of the nozzle. The pressure fields induced by the streamwise jets were quite different. The primary effect was a low-pressure region which spread laterally from the sides of the jet. There was almost no wake and only a small region of positive pressure forward of the nozzle exit. The third part of Fig. 6 gives C_p contours of a circular jet at $R = 4.0$ and $\delta_j = 90$ deg.[7] Comparisons of the three distributions show that the rectangular jet distributions tend, in a qualitative sense, to "bracket" the circular jet results. The circular jet had a low-pressure wake region similar to that exhibited by the blunt rectangular jet, while the lateral spread of low pressure and small upstream positive-pressure region are more characteristic of streamwise-oriented rectangular jets.

The influence of velocity ratio R on the induced pressure fields is illustrated in Fig. 7. This figure indicates that velocity ratio has three principal effects: 1) the total area affected by the interaction increases as R increases; 2) the negative pressure field expands forward and outward as R increases, while the positive pressure field contracts (Note movement of $C_p = 0$ contour in Fig. 7.); 3) the pressure gradients tend to steepen with increasing R, particularly in the negative pressure region. The above comments also apply to distributions induced by streamwise jets, but on a smaller scale. (Streamwise jets do not seem to generate quite as large induced effects as do the blunt jets.)

Jet Centerline Location

The procedures used to determine the jet centerline location data were described in a previous section. The U_v component was fitted with a parabolic curve, as illustrated in Fig. 4. The point corresponding to zero slope was then taken as the local jet centerline location, and these coordinates were transformed to the X, Y, Z coordinate system (Fig. 3). Since the measurements were made at several X locations along the jet centerline trajectory, a set of $\{x,z\}$ values was developed for each R-δ_j combination and each nozzle orientation. As shown

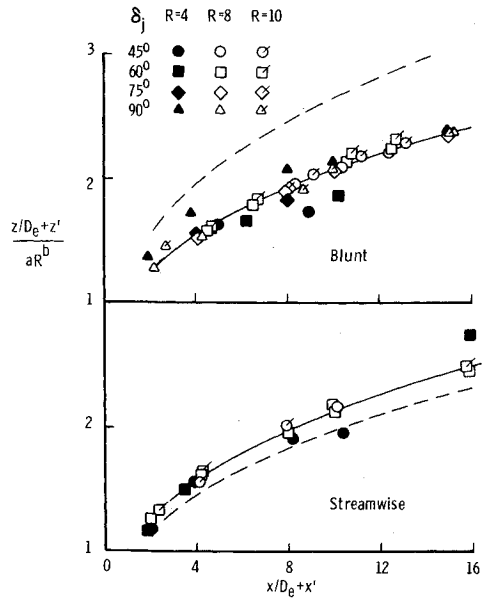

Fig. 8 Accuracy of jet centerline curve fits. (Dashed lines are circular jet results for $R=8$ from Ref. 5.)

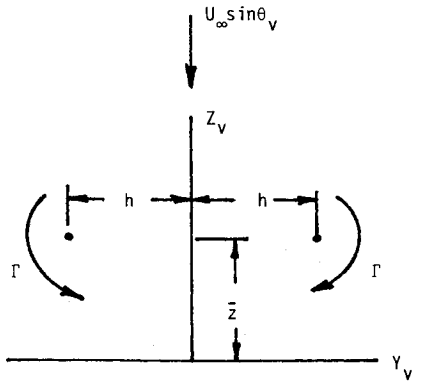

Fig. 9 Coordinate system for filament vortex fit.

by Fearn and Weston,[5] these data can easily be fitted by a power equation of the form

$$z/D_e = aR^b (x/D_e + x')^c - z' \tag{1}$$

where a, b, and c are fit parameters and x' and z' are given by

$$x' = (\tan\delta_e / ac R^b)^{1/(c-1)} \tag{2}$$

with

$$\delta_e = 90 + d(90-\delta_j) + e(90-\delta_j)^2$$

$$z' = aR^b x'^c \tag{3}$$

Table 2 Fit parameters

Nozzle configuration	Jet centerline a	b	c	d	e
Blunt	0.7947	0.9120	0.3190	0.02458	−0.02351
Streamwise	1.540	0.7345	0.3293	−0.2486	0.0
	Vortex curve				
Blunt	0.2105	1.237	0.4131	−0.09306	−0.02681
Streamwise	0.9378	0.8109	0.3394	−0.1383	0.0

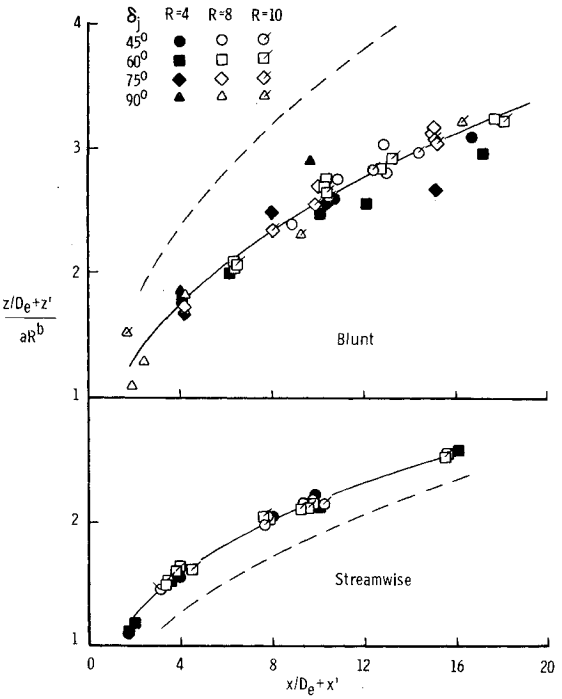

Fig. 10 Accuracy of vortex curve fits. (Dashed lines are circular jet results for $R=8$ from Ref. 5.)

where $x' = z' = 0$ for $\delta_j = 90$ deg. Values of a, b, c, d, and e are given in Table 2. The accuracy of the fits is illustrated in Fig. 8.

Vortex Curve Location

The vortex curve is defined as the projection of the vortex trajectories onto the symmetry plane (Fig. 3). The procedures used to locate the vortex curve were described in a previous section. The impetus for this procedure arises from consideration of the upwash field (in the symmetry plane, Fig. 3) generated by two infinite filament vortices (Fig. 9). This expression is given by

$$W_v = \Gamma h / \{\pi[h^2 + (z_v - \bar{z})^2]\} - U_\infty \sin\theta_v \tag{4}$$

where θ_v is the angle between the Z_v and Z axes and the remaining parameters are defined in Fig. 9. It is easily verified that the maximum W_v occurs for $z_v = \bar{z}$. Given a set of W_v data in the symmetry plane, the method of differential corrections was used to fit these data using Eq. (4), with Γ, h, and $\bar{z}$ as the unknown parameters. A sample result is shown in Fig. 4. The vortex curve was assumed to lie at the peak in the curve fit. Given this set of $\{x,z\}$ values determined in this fashion, a power curve of the form given in Eqs. (1-3) can be fitted to these data. Values of the associated fit parameters are provided in Table 2, and the relative accuracy of the fit is depicted in Fig. 10. The applicable circular jet results (dashed curves) are provided for comparison purposes.

Determination of h *and* Γ

Although the filament fitting process described above does provide values of h and Γ, these values can sometimes be unreliable. The principal cause of these discrepancies is that since the fit is proportional to Γh [Eq. (4)], one can alter the values of each while keeping the product a constant. The result is that the fit can actually be quite good while the values of h and Γ can be somewhat absurd. Apparently, a more reliable, less sensitive fit procedure is needed to extract h and Γ from the data.

Following the lead of Fearn and Weston,[5] the so-called diffuse or Lamb[9] vortex model was chosen for analysis. In

this model, each of the contrarotating vortices is assumed to have a Gaussian vorticity distribution. Thus

$$\omega = \omega_0 \exp(-\beta^2 r^2)$$

The total vorticity is then (Fig. 11)

$$\omega = \omega_0 [\exp(-\beta^2 r_1^2) - \exp(-\beta^2 r_2^2)] \tag{5}$$

and the total velocity vector (V) at any point is given by superposition as

$$V = \frac{\Gamma_0}{2\pi}\left[\left(\frac{1-\exp(-\beta^2 r_1^2)}{r_1}\right)e_1 - \left(\frac{1-\exp(-\beta^2 r_2^2)}{r_2}\right)e_2\right]$$

$$- U_\infty \sin\theta_v e_3 \tag{6}$$

where Γ_0 is the total integrated strength

$$\Gamma_0 = \int_0^{2\pi}\int_0^{\infty} \omega_0 \exp(-\beta^2 r^2) r\,dr\,d\theta = \pi\omega_0/\beta^2 \tag{7}$$

Since, in general, vorticity may be cancelled by diffusion across the symmetry plane, the effective strength of each vortex was taken as the flux of vorticity across the half-plane $Y_v \leq 0$

$$\Gamma = \int_{-\pi/2}^{\pi/2}\int_0^{\infty} \omega r\,dr\,d\theta \tag{8}$$

where ω is given by Eq. (5). Similarly, the effective vortex spacing h is given by

$$h = \frac{1}{\Gamma}\int_{-\pi/2}^{\pi/2}\int_0^{\infty} Y_v \omega r\,dr\,d\theta \tag{9}$$

Since Eq. (6) is a vector equation, one may choose to fit any one or all of the components. Fearn and Weston chose the W_v component; the same procedure was followed in the current study. There are two advantages associated with using the Lamb model. First, the model is more physically reasonable than the filament model. Second, the data base to which the model is fitted is quite large. (The lateral vortex sweep data are used, Fig. 5.) Not only is there more information about the details of the flow structure in these data, but also small data measurement errors have less effect on the fit parameters.

Vortex strength data and samples of the vortex spacing data extracted from both the filament and Lamb models are presented in Figs. 12–14. Vortex spacing does not vary appreciably with δ_j.

Faired Body Test Results

The purpose of the faired body test series was to obtain data on relatively shallow angle jets (15 deg $\leq \delta_j \leq$ 45 deg). A

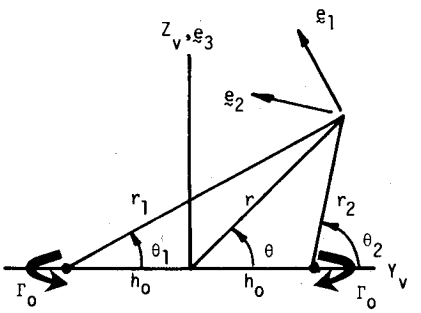

Fig. 11 Coordinate system for Lamb vortex fit.

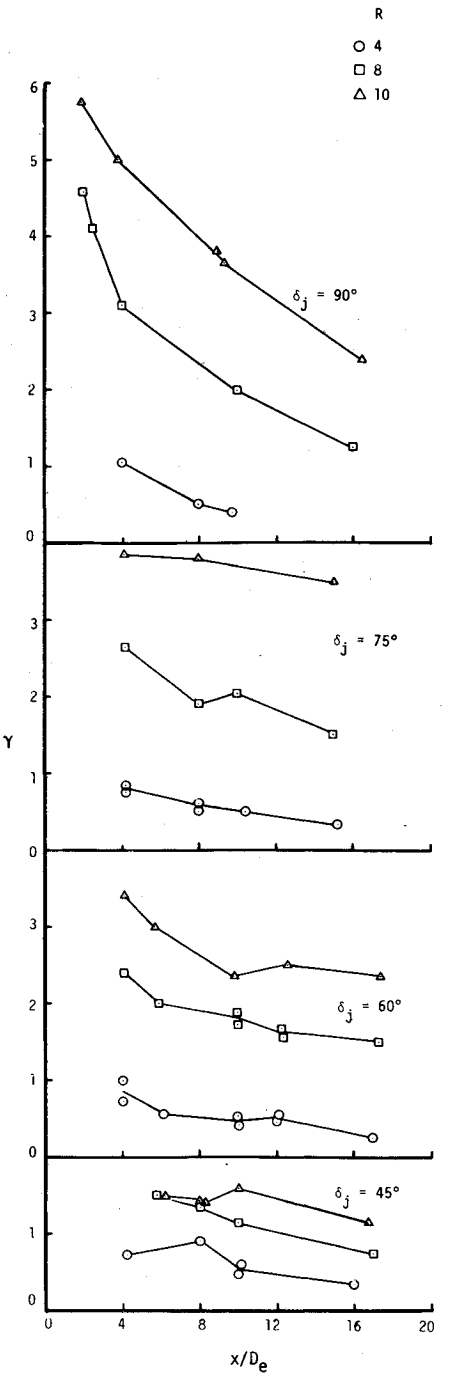

Fig. 12 Vortex strength for blunt nozzles; reflection plane data.

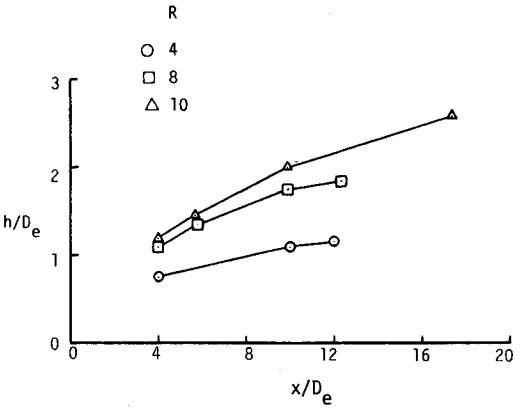

Fig. 13 Vortex spacing data for 60 deg blunt nozzle.

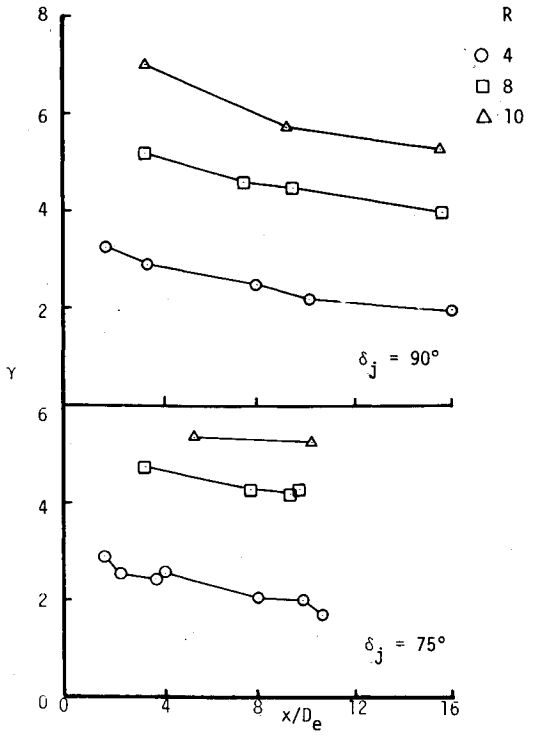

Fig. 14 Vortex strength for streamwise nozzles; reflection plane data.

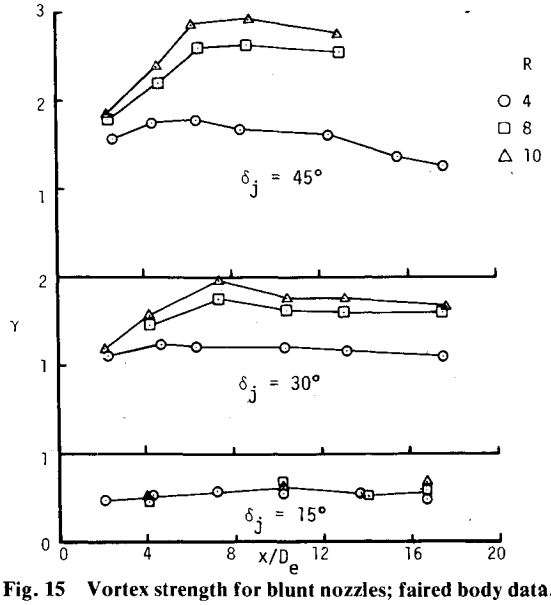

Fig. 15 Vortex strength for blunt nozzles; faired body data.

significant effort was devoted to the design of the faired body itself in order to provide a relatively interference-free structure. The design was constrained by the existence of the fixed air supply hardware. A photograph of the installation is given in Fig. 2.

Detailed jet and vortex flowfield properties were measured at three injection angles (Table 1). No surface static pressure data were measured. The data analysis procedures outlined in the previous sections were applied; the Γ distributions are given in Fig. 15. (Again, the h distributions are somewhat repetitive.)

Comparison of Reflection Plane and Faired Body Data

The Γ distributions (for the 45 deg jet at $R=4$) from the reflection plane and faired body tests are compared in Fig. 16. The comparison indicates that the data agree neither in a qualitative nor a quantitative sense. This is an extremely

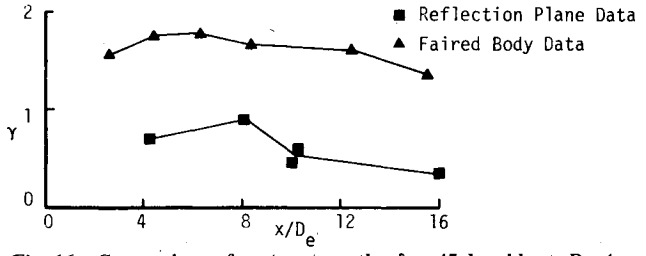

Fig. 16 Comparison of vortex strengths, $\delta_j = 45$ deg, blunt, $R=4$.

disturbing result. It implies that changes in the jet exit configuration can dramatically alter the nature of the jet/crossflow interaction and its induced effects. It should be recognized that the faired body was designed to minimize flow separation on its surface. It is possible that, as the jet interaction occurs, local flow change can induce local circulation patterns.

In addition, these discrepancies imply that the reflection plane installation, on which almost all jet-in-crossflow data have been obtained, is not as "inert" a test bed (i.e., boundary condition) as had been assumed over the years. It is the authors' opinion that the differences in vortex data should diminish as the jet injection angle is increased. This opinion is based on the premise that the plate geometry interferes with the initial formation of the vortices, thus diffusing their strength. Whatever the cause, the results outlined above do indicate a pressing need for more basic research in the jet/crossflow interaction field, particularly for practical aircraft configurations.

IV. Conclusions

The following conclusions may be drawn from the current study:

1) The crossflow penetration and vortex strengths of the blunt-oriented jets are less than those of the streamwise-oriented jets, at the same injection angle and velocity ratio.

2) The induced effects of blunt and streamwise jets differ quite dramatically. The blunt jet induced effects are more pronounced in both magnitude and extent.

3) The induced effects and nominal vortex properties[10] of the streamwise-oriented jets compare quite well with similar effects/properties of circular jets. The blunt jets exhibit quite different properties.

4) The unfavorable comparison of flowfield data taken on different test installations at similar nozzle exit conditions suggests the pressing need for more basic research into the jet/crossflow interaction.

References

[1] Pratte, B.D. and Baines, W.D., "Profiles of the Round Turbulent Jet in a Crossflow," *Journal of the Hydraulics Division, Proceedings of the ASCE,* Vol. 92, Nov. 1967, pp. 53-64.

[2] "Analysis of a Jet in a Subsonic Crosswind," NASA SP-218, 1969.

[3] Thompson, A.M., "The Flow Induced by Jets Exhausting Normally From a Plane Wall into an Airstream," Ph.D. Thesis, University of London, London, England, 1971.

[4] Kamotani, Y. and Greber, I., "Experiments on a Turbulent Jet in a Crossflow," *AIAA Journal,* Vol. 10, Nov. 1972, pp. 1425-1429.

[5] Fearn, R. and Weston, R.P., "Vorticity Associated with a Jet in a Crossflow," *AIAA Journal,* Vol. 12, Dec. 1974, pp. 1666-1671.

[6] Fearn, R.L. and Weston, R.P., "Induced Velocity Field of a Jet in a Crossflow," NASA TP 1087, 1978.

[7] Fearn, R.L. and Weston, R.P., "Induced Pressure Distribution of a Jet in a Crossflow," NASA TN D-7916, 1975.

[8] Weston, R.P., "A Description of the Vortex Pair Associated with a Jet in a Crossflow," Presented at the Navy Workshop on Prediction Methods for Jet V/STOL Aerodynamics, July 1975.

[9] Lamb, H., *Hydrodynamics,* 6th ed., Dover, New York, 1932, pp. 591-592.

[10] Krausche, D., Fearn, R.L., and Weston, R.P., "Round Jet in a Crossflow: Influence of Injection Angle on Vortex Properties," *AIAA Journal,* Vol. 16, June 1978, pp. 636-637.